An Active Dynamic Vibration Absorber for a Hand-Held Vibro-Elastography Probe

Hassan Rivaz
e-mail: rivaz@jhu.edu

Robert Rohling[1]
e-mail: rohling@ece.ubc.ca

Department of Electrical and Computer Engineering,
University of British Columbia,
2332 Main Mall,
Vancouver, BC, Canada, V6T1Z4

Vibro-elastography is a new medical imaging method that identifies the mechanical properties of tissue by measuring tissue motion in response to a multi-frequency external vibration source. Previous research on vibro-elastography used ultrasound to measure the tissue motion and system identification techniques to identify the tissue properties. This paper describes a hand-held probe with a combined vibration source and ultrasound transducer to implement the new method as a practical device. The device uses a proportional integral active dynamic vibration absorber with an electromagnetic actuator to counterbalance the reaction forces from contact with the tissue. Experiments show an operational frequency range of 5–20 Hz*, with at least* 15 dB *vibration absorption in* 0.4 s *for single frequency excitation. Experiments with variable frequency and amplitude excitation also show a high level of vibration absorption.* [DOI: 10.1115/1.2424982]

1 Introduction

1.1 Problem Statement and Need for Vibration Absorption. Elastography, the pixel-based display of the spatial variation of elastic modulus of tissue, is an emerging medical imaging method. Depending on the complexity of the tissue model, an elastogram can be obtained in real time or offline. One motivation for elastography is that tissue abnormalities are often correlated to a local change in their mechanical properties. For example, roughly one-half of breast cancers detected in the United States are first discovered by the patient feeling a hard lump in her breast [1]. Currently, manual palpation is widely used to examine breast abnormalities. Unfortunately, this technique is subjective and is limited to lesions near the skin surface [2]. To overcome this problem, elastography can be used to aid the detection and quantification of tumors. In particular, medical ultrasound imaging equipment is used to measure tissue motion in response to compression (a simple illustrative example is shown in Fig. 1). From the ultrasound images, the local mechanical properties of tissue can be determined and displayed as an image (elastogram).

Vibro-elastography (VE) is a recent variation of elastography that vibrates tissue externally over a range of low-frequency vibrations [3–5]. In VE, multiple ultrasound images are captured while the tissue is vibrating, and each image is compared to the previous image to provide a grid of local displacement measurements. These displacement fields are then used to determine the visco-elastic properties of the tissue at each grid location. The grid of calculated visco-elastic properties can be displayed as an image. What makes VE different from other elastography methods is that the tissue response at different frequencies and different time instances are obtained and that tissue properties are calculated from the combined set of these measurements. Normally only the tissue elasticity is obtained, but the VE method also has the potential to extract viscosity and density from the dynamic response of tissue.

Currently, the VE method has been demonstrated using bench top approaches [4]. Clinical acceptance of vibro-elastography would be aided by the development of a hand-held probe that includes both the imaging device (the ultrasound probe) and an excitation source that vibrates the tissue. Figure 2(*a*) shows an early proposal for such a hand-held device. Two actuators jointly vibrate tissue and the attached ultrasound probe images the tissue motion.

For a hand-held probe, the reaction forces between the tissue and vibrator act as an external disturbance on the probe assembly and will cause unwanted vibration of it. These vibrations should be minimized to maintain the comfort of the operator and the accuracy of the VE calculations. Therefore, the probe design should use some form of vibration absorption. Since the desirable sweep rate for VE is still largely unknown, it is desirable to have a system with the fastest response and widest range as possible. To cover a reasonable bandwidth of tissue response in our current vibro-elastography system, the device should be operational in a 5–25 Hz frequency range. VE can be performed by vibrating the tissue with an excitation sweeping the 5–25 Hz frequency range in a time interval as small as 3 s. To achieve reasonable vibration absorption, however, we perform the sweep in a longer period of time, say 10 s.

Held by hand, the probe can move in all six degrees of freedom. The operator's hand is also a distributed mass system that vibrates around the nonlinear visco-elastic joints at wrist, elbow, and shoulder. Since the amplitude of tissue excitation is small, so are the reaction forces exerted on the device and its vibration amplitude. The greatest motion is axial. Therefore the hand-held device can be modeled as a 1 degree of freedom (DOF) linear mass–spring–damper system (Fig. 2(*b*)). The combination of the device and the operator's hand will be referred to as the primary system.

1.2 Vibration Reduction Approach. Five different possible methods for reducing the vibration of the hand-held device are shown in Fig. 3: vibration isolation, semi-active vibration isolation, passive dynamic vibration absorption (DVA), semi-active DVA, and active DVA. Reference [6] provides a survey of vibration isolation methods, Ref. [7] has a fairly complete list of DVA variations, reference Ref. [8] provides an overview of DVA applications and semi-active DVA methods, and reference Ref. [9] reviews semi-active vibration isolations and semi-active DVA's and their applications. Vibration isolators, due to the need for a reasonably stiff connection to the actuator, only provide vibration isolation for high-frequency excitations [10]. Passive DVA provides vibration absorption by using an additional absorber mass but operates at a single or narrow band of frequencies. To overcome this problem, multiple DVA's [11] and beam structures [12] have been used to cancel excitations with multiple frequencies.

[1]Corresponding author.

Contributed by the Technical Committee on Vibration and Sound of ASME for publication in the JOURNAL OF VIBRATION AND ACOUSTICS. Manuscript received February 27, 2006; final manuscript received September 21, 2006. Assoc. Editor: D. Dane Quinn.

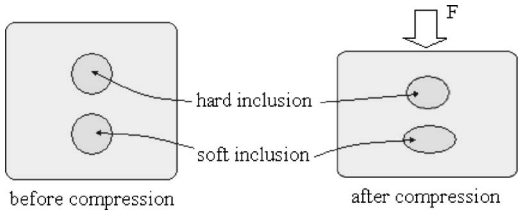

Fig. 1 Hard and soft inclusions are subject to an external compression (*F*)

Another class of vibration absorbers is nonlinear DVA. A pendulum connected to the primary system is considered a nonlinear vibration absorber. For a rotary primary system such as automobile engine, a pendulum can act as a wideband vibration absorber [10]. For a linear primary system, a pendulum vibration absorber [13] has a narrow operational frequency range. Multiple pendulums are proposed to widen the operational frequency [14]. The pendulum, however, applies forces in directions perpendicular to the excitation force. Even though these forces are very small, motion of the probe parallel to the skin (or rotation) introduces difficulties in the elastography application.

Examples of hand-held devices with vibration absorption covering a range of frequencies are rare. For example in Ref. [15], vibration isolation and DVA are combined to provide vibration protection for an operator of a hand-held percussion machine. In that work, the vibration isolator reduces the high frequency components of acceleration perceived by the operator, and the DVA suppresses the specific harmonics of machine acceleration.

Since tissue must be excited over a range of low frequencies in VE, semi-active, multiple DVAs or active methods should be used. Semi-active and multiple DVA methods only provide partial vibration reduction because of their damping component. Given the need for a high level of vibration reduction, and the constraints of weight, size and cost, active DVA is selected for the hand-held VE device.

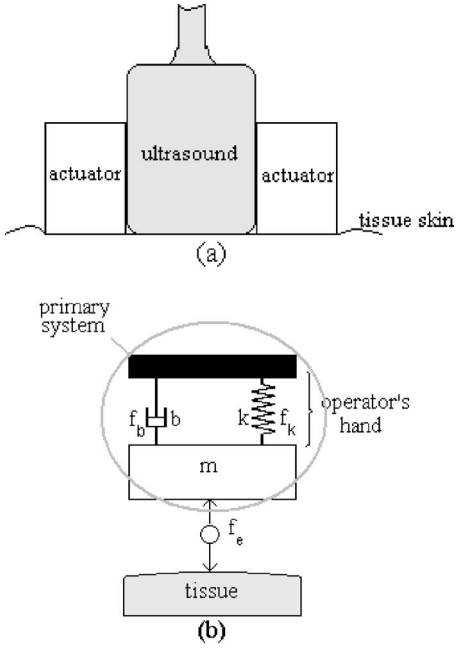

Fig. 2 (*a*) A hand-held device for VE; and (*b*) mass-spring-damper model of the device held by hand. The term primary system refers to the combined effective mass, stiffness and damping of the hand held assembly, i.e., including the operator. f_k and f_b are the external forces from the hand.

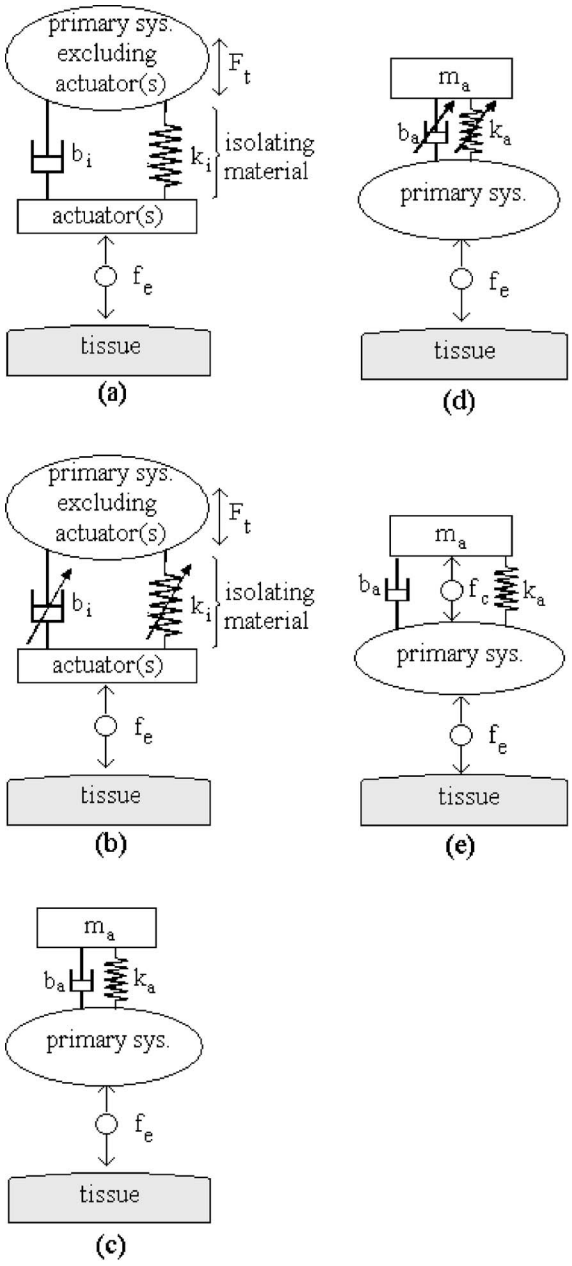

Fig. 3 (*a*) Vibration isolation; (*b*) semi-active vibration isolation; (*c*) passive dynamic vibration absorption (DVA); (*d*) semi-active DVA; and (*e*) active DVA

1.3 Active DVA Control. Active DVA control algorithms can be grouped into two categories. The first category comprises algorithms that require *full system* analysis. Examples include H_∞ optimal control [16], H_2 optimal dynamic absorber [17], bandpass vibration absorber [18], delayed feedback vibration absorber [19], and linear quadratic Gaussian (LQG) active vibration control [20]. Such design approaches cannot be used for the hand-held device because the probe can be held by various operators with different inertia, damping, and stiffness properties. The properties of the system whose vibration is to be cancelled can therefore change substantially. Most of these optimal control approaches provide an automatic search strategy for the properties of the primary and absorber system that provide the best vibration absorption performance. However, they still require a "good" estimate of these properties as a starting point, which cannot be provided in clinical practice.

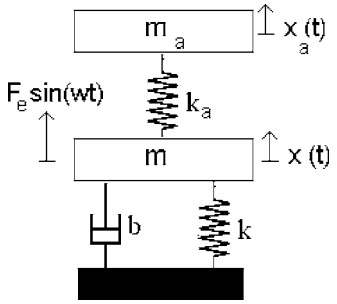

Fig. 4 DVA with zero damping attached to the primary system

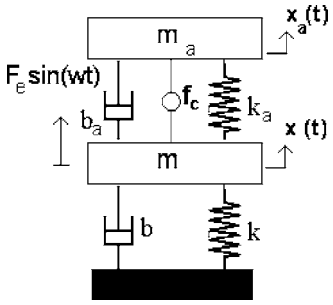

Fig. 5 Active DVA attached to the primary system

Algorithms in the second category consist of methods whose control law is decoupled from the primary system and does not require any knowledge of it. These methods use the vibration absorption capability of a mass—spring system (DVA with zero damping). Two such implementations of active DVA are the delayed resonator (DR), introduced by Olgac and Holm-Hansen in 1993 [21], and the proportional integrator (PI) controller, developed in this work. The DR is easy to implement and requires only one feedback from the system. However, its operational frequency is bound by both lower and upper limits when an electromagnetic actuator is used to apply the control force [22]. Before describing the new PI controller, a review of DVA with zero damping is given.

1.4 DVA With Zero Damping. Figure 4 shows a DVA with zero damping attached to a 1 DOF system. The transfer function between the displacement of the device x and the excitation force f_e is

$$\frac{X(s)}{F_e(s)} = \frac{m_a s^2 + k_a}{m m_a s^4 + b m_a s^3 + (k_a m + k m_a + k_a m_a) s^2 + b k_a s + k k_a} \tag{1}$$

where m, k, and b are, respectively, the mass, damping, and stiffness of the primary system, and m_a and k_a are, respectively, the mass and stiffness of the absorber. The Laplace transform of variables are capitalized.

Suppose that the excitation force f_e has frequency ω_e. The absorber system is said to be *tuned* to the excitation frequency if $k_a = m_a \omega_e^2$. Equation (1) indicates that the steady-state value of x is zero at that frequency, giving perfect vibration absorption [10]. Such a DVA with zero damping is not practically realizable. Other peak response frequencies are also introduced in the system. So the frequency of the excitation should be kept within the very small frequency range that the passive DVA is designed for. Active DVA solves both of these problems by applying an additional control force (Fig. 3(*e*)).

In the next section, a new formulation is derived based on PI control and a single feedback. The design of the hand-held device is presented next. Stability and transient response of the combined system are studied next. Simulation and experimental results are provided, verifying the theory of the method and the stability analysis. A discussion of practical issues follows.

2 PI-DVA Formulation

A PI controlled active DVA (PI-DVA) with acceleration feedback is now developed for an electromagnetic actuator. For an intuitive view of the controller we start with a simple model neglecting actuator dynamics and assuming smooth acceleration measurements with zero drift. Figure 5 shows the PI-DVA attached to the primary system, obtained by combining Figs. 2(*b*) and 3(*e*). The control force, f_c, of a PI controller with acceleration feedback has the form

$$f_c = K_p \ddot{x}_a + K_i \dot{x}_a \tag{2}$$

where K_p and K_i are the proportional and integral gain coefficients respectively; and x_a is the position of the absorber mass. Having this force as the control command, the equation of motion of the absorber mass is

$$m_a \ddot{x}_a + b_a \dot{x}_a + k_a x_a = K_p \ddot{x}_a + K_i \dot{x}_a \tag{3}$$

Taking the Laplace transform, one has

$$m_a s^2 + b_a s + k = K_p s^2 + K_i s \tag{4}$$

By selecting the K_p and K_i such that the roots of the above equation are placed on the imaginary axis at $\pm j\omega_e$, the absorber system will mimic a resonator at the frequency of ω_e. This system can perfectly cancel the vibrations of the primary system at the frequency ω_e (Eq. (1)). Solving Eq. (4) with $s = \pm j\omega_e$ gives

$$K_p = m_a - k_a/\omega_e^2 \text{ and } K_i = b_a \tag{5}$$

Actuator dynamics and filters are added next.

2.1 PI-DVA With Electromagnetic Actuator. A linear electromagnetic actuator is chosen to apply the control force because it can provide actuation over a wide frequency at a low cost. The block diagram representation of the controller with filters is shown in Fig. 6. To obtain the velocity data from the acceleration data, a first-order Butterworth highpass filter with a 0.5 Hz cutoff frequency is used before integration to eliminate the low-frequency drift of the accelerometer data. The integration is performed in the software. To remove the high-frequency components from the first term of the control force ($K_p \ddot{x}_a$), the accelerometer data is lowpass filtered before feeding it to the proportional gain term. An 80 Hz first-order Butterworth filter is used here. The dynamic equations of the system are

$$m_a \ddot{x}_a(t) + b_a \dot{x}_a(t) + k_a x_a(t) = K_f i(t) \tag{6}$$

$$L\dot{i}(t) + Ri(t) + K_b \dot{x}_a(t) = K_p \ddot{x}_a + K_i \dot{x}_a \tag{7}$$

where i is the current; L and R are the inductance, and the dc resistance; and K_f and K_b are the force sensitivity and back emf constants of the actuator. Taking the Laplace transform and including the filters gives

$$\overbrace{\begin{bmatrix} m_a s^2 + b_a s + k_a & -K_f \\ K_b s - F_{\text{lp}} s^2 K_p - F_{\text{hp}} s K_i & Ls + R \end{bmatrix}}^{G(s)} \begin{bmatrix} X_a(s) \\ I(s) \end{bmatrix} = 0 \tag{8}$$

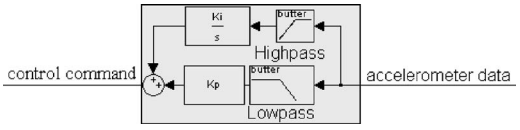

Fig. 6 Block diagram representation of the PI controller

where $F_{\text{lp}}=\omega_{lp}/(s+\omega_{\text{lp}})$ and $F_{\text{hp}}=s/(s+\omega_{\text{hp}})$ are the lowpass and highpass filters, respectively. The characteristic equation of the system is obtained by setting $\det|G(s)|=0$

$$A(s)-\omega_{\text{lp}}(s+\omega_{\text{hp}})K_p-(s+\omega_{\text{lp}})K_i=0 \tag{9}$$

where

$$A(s)=[(m_a s^2+b_a s+k_a)(Ls+R)+K_f K_b s](s+\omega_{\text{lp}})(s+\omega_{\text{hp}})/(K_f s^2) \tag{10}$$

The characteristic equation should have two roots at $\pm j\omega_e$ in order for the PI-DVA to mimic the mass–spring resonator of Fig. 4. Setting $s=\pm j\omega_e$ in Eq. (9) and solving for its real and imaginary parts, K_p and K_i can be found as

$$K_p=\frac{-\omega_e \operatorname{Re}\{A(s)\}_{s=j\omega_e}+\omega_{\text{lp}} \operatorname{Im}\{A(s)\}_{s=j\omega_e}}{\omega_{\text{lp}}\omega(\omega_{\text{lp}}-\omega_{\text{hp}})} \tag{11}$$

$$K_i=\frac{\omega_e \operatorname{Re}\{A(s)\}_{s=j\omega_e}-\omega_{\text{hp}} \operatorname{Im}\{A(s)\}_{s=j\omega_e}}{\omega(\omega_{\text{lp}}-\omega_{\text{hp}})} \tag{12}$$

If the operational frequency is such that s/ω_{lp} and $\omega_{\text{hp}}\ll s\leqslant 1$, Eqs. (11) and (12) can be simplified to

$$K_p=\frac{\omega_e \operatorname{Re}\{A'(s)\}_{s=j\omega_e}+\omega_{\text{hp}} \operatorname{Im}\{A'(s)\}_{s=j\omega_e}}{K_f\omega_e^3} \tag{13}$$

$$K_i=\frac{\omega_e \operatorname{Re}\{A'(s)\}_{s=j\omega_e}+\omega_{\text{lp}} \operatorname{Im}\{A'(s)\}_{s=j\omega_e}}{K_f\omega_e} \tag{14}$$

where $A'(s)$ is defined as

$$A'(s)=(m_a s^2+b_a s+k_a)(Ls+R)+K_f K_b s \tag{15}$$

The simplified version can be used when real-time retuning is required, like in swept-sine excitation, and the processor is not fast enough to perform the calculations of Eqs. (11) and (12).

3 Stability of the Combined System

Although it is guaranteed that the PI controller makes the absorber system marginally stable, the stability of the combined system should be investigated. The dynamic equations can be written as

$$m\ddot{x}(t)+(b+b_a)\dot{x}(t)+(k+k_a)x(t)-b_a\dot{x}_a(t)-k_a x_a(t)=f_e-K_f i(t) \tag{16}$$

$$m_a\ddot{x}_a(t)+b_a\dot{x}_a(t)+k_a x_a(t)-b_a\dot{x}(t)-k_a x(t)=K_f i(t) \tag{17}$$

$$L\dot{i}(t)+Ri(t)+K_b\dot{x}_a(t)-K_b\dot{x}(t)=K_p\ddot{x}_a+K_t\dot{x}_a \tag{18}$$

Taking the Laplace transform, one obtains

$$\overbrace{\begin{bmatrix} ms^2+(b+b_a)s+(k+k_a) & -(b_a s+k_a) & K_f \\ -(b_a s+k_a) & m_a s^2+b_a s+k_a & -K_f \\ -K_b s & K_b s-(F_{\text{lp}}s^2K_p+F_{\text{hp}}sK_i) & Ls+R \end{bmatrix}}^{H(s)} \times\begin{bmatrix} X \\ X_a \\ I \end{bmatrix}=\begin{bmatrix} F_e \\ 0 \\ 0 \end{bmatrix} \tag{19}$$

where again F_{lp} and F_{hp} are the lowpass and highpass filters, now written explicitly. The characteristic equation of the system is obtained by setting $\det|H(s)|=0$

$$B(s)+\omega_{\text{lp}}(s+\omega_{\text{hp}})K_p+(s+\omega_{\text{lp}})K_i=0 \tag{20}$$

where

$$B(s)=N(s)(s+\omega_{\text{lp}})(s+\omega_{\text{hp}})/K_f s^2(ms^2+bs+k) \tag{21}$$

and

$$N(s)=(ms^2+bs+k)[(m_a s^2+b_a s+k_a)(Ls+R)+K_f K_b s]+m_a s^2[(Ls+R)(b_a s+k_a)+K_f K_b s] \tag{22}$$

Equations (11) and (12) give the K_p and K_i values as a function of frequency of excitation. These values should be inserted into Eq. (20) in order to investigate the stability of the combined system. Several methods can be employed to investigate the stability of Eq. (20); here we use the "D-subdivision" stability method [23]. To use this method, the marginal stability of the combined system should be studied. Setting $s=\pm j\omega_c$ in Eq. (20), where subscript c refers to the combined system, we obtain

$$K_p=\frac{\omega_c \operatorname{Re}\{B(s)\}_{s=j\omega_c}-\omega_{\text{lp}} \operatorname{Im}\{B(s)\}_{s=j\omega_c}}{\omega_c\omega_{\text{lp}}(\omega_{\text{lp}}-\omega_{\text{hp}})} \tag{23}$$

$$K_i=\frac{-\omega_c \operatorname{Re}\{B(s)\}_{s=j\omega_c}+\omega_{\text{hp}} \operatorname{Im}\{B(s)\}_{s=j\omega_c}}{\omega_c(\omega_{\text{lp}}-\omega_{\text{hp}})} \tag{24}$$

These equations will be referred to later when investigating the stability of the actual device.

4 Hand-Held Probe and Combined System

Figure 7 shows the hand-held device. Parts labeled as (*a*), (*c*), and (*d*) are the moving head which vibrates tissue, the slide rods, and the CNC machined aluminum shell, respectively. Parts (*g*) and (*h*) are the primary actuator's (LA-14-17-000 A, BEI Kimco, San Marcos, USA) coil and magnet. This actuator vibrates the tissue, while the ultrasound probe (*b*) images the tissue. The absorber actuator is mounted in an opposite way: its coil (*j*) is fixed and the magnet (*k*) moves. Therefore, the absorber mass is simply the magnet of the actuator. This choice eliminates the need for an additional absorber mass, making the hand-held device lighter. Part (*l*) is one of the two absorber springs. Parts (*f*) and (*i*) are a linear potentiometer (LCP8S-10, ETI Systems, Carlsbad, USA) and a piezoelectric accelerometer (4508-002, Bruel and Kjaer, Naerum, Denmark), respectively. The accelerometer is mounted on the absorber mass (the magnet) and provides the only feedback for the vibration absorption algorithm. The potentiometer signal is only used to operate the first actuator under closed loop control for displacement control. Here a conventional PID controller is used. Since the mathematical model of the vibrator is unknown, the coefficients of the PID controller are obtained by the Ziegler–Nicholas method [24]. To prevent the magnetic fields of the two linear actuators interfering, especially since the absorber mass (*k*) is the magnet, a hollow spacer (*e*) is placed between them.

The natural frequency of the absorber $\omega_{\text{na}}=\sqrt{k_a/m_a}$ is selected by minimizing the maximum of the control force in the 5–25 Hz

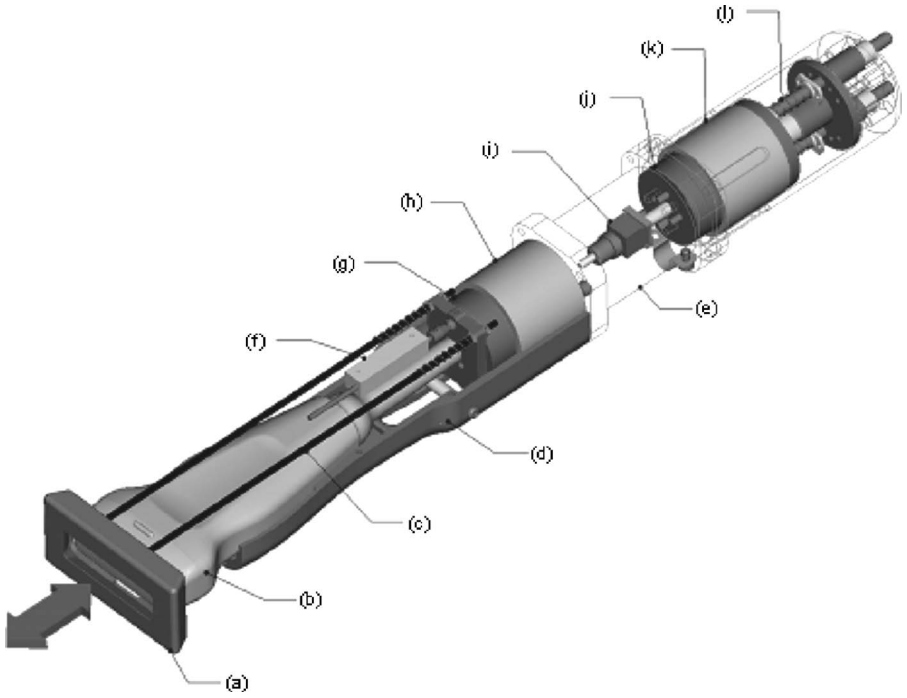

Fig. 7 Exploded view of the hand-held probe: (*a*) moving head; (*b*) ultrasound probe; (*c*) slide rod; (*d*) machined shell; (*e*) spacer; (*f*) linear potentiometer; (*g*) and (*h*) primary actuator's coil and magnet; (*i*) accelerometer; (*j*) and (*k*) absorber actuator's coil and magnet; and (*l*) absorber spring

operational range, resulting in $\omega_{na}=9$ Hz. We also set[2] $m_a=0.2$ kg and therefore $k_a=m_a\omega_{na}^2=637$ N/m. The Coulomb friction and the Eddy currents induced by the moving magnet in the housing and the coil are the sources of damping, i.e., no damper is used in the PI-DVA. Using the free vibration test results, the damping coefficient in the absorber system was calculated to be $\zeta_a=0.16$, or equivalently, $b_a=3.6$ kg/s. Because of the nonlinear source of the damping, its value can be frequency dependent [10]. In order to find this dependency, the absorber system was tuned to resonate at different frequencies and the b_a was manually varied over an interval around 3.6 kg/s. It was observed that the b_a value changes slightly with the tuning frequency. A lookup table relating the tuning frequency and b_a was obtained in order to optimize performance as the operational frequency changes. This also roughly takes into account the possible errors of actuator parameters. When producing the look up table, it is ensured that the absorber system is slightly dissipative. This results in a stability margin against the uncertainties in the system. There is, of course, a tradeoff between the stability margin and the performance of the vibration absorption.

The primary system properties are $m=1$ kg, $k=140$ N/m, $b=4$ kg/s ($\zeta=0.16$). These properties depend on how the probe is held and also on the operator. The mass of the whole hand-held device (excluding the absorber mass) is approximately 0.5 kg, and it is assumed that the effective mass of the operator's hand is another 0.5 kg.[3] To obtain k, the probe was held by different subjects and different grabbing forces and an external load was applied to the probe. The deflection of the hand was then measured and the stiffness was calculated.[4]

[2]This value is the mass of the magnet of the electromagnetic actuator.

[3]Since the hand is a distributed mass system and vibrates around the arthroses at wrist, elbow and shoulder, the effective mass is only a percentage of the whole mass of the hand. As an example, for a rod with uniform mass distribution that rotates around a hinge at one of its ends, the effective mass is 1/3 of the total mass.

[4]These values of the properties of the primary system will be allowed to vary over a certain range, since they vary for different persons holding the device.

5 Operational Frequency Range of the Combined System

Figure 8 shows the plot of K_p versus K_i for both the absorber system and the combined system. In this figure, the properties of

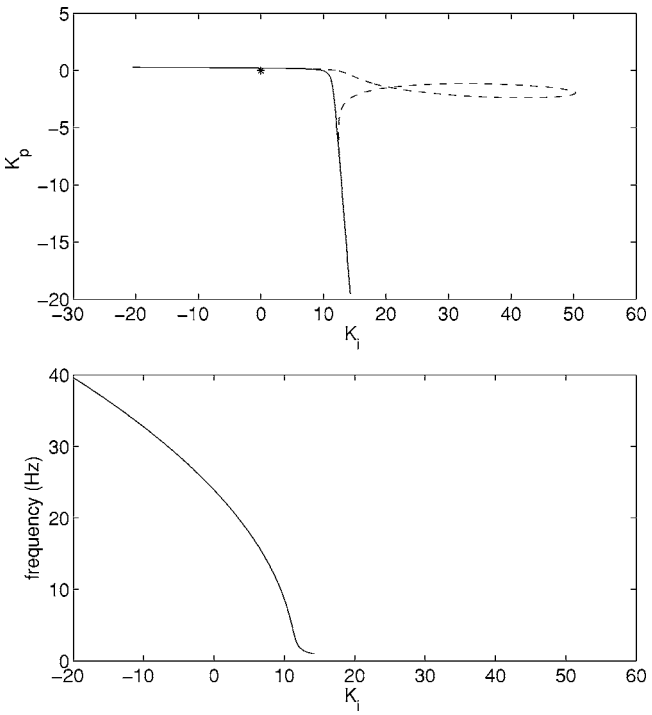

Fig. 8 Stability chart. K_p and frequency versus K_i. The dashed and solid curves correspond to the combined system and absorber system, respectively.

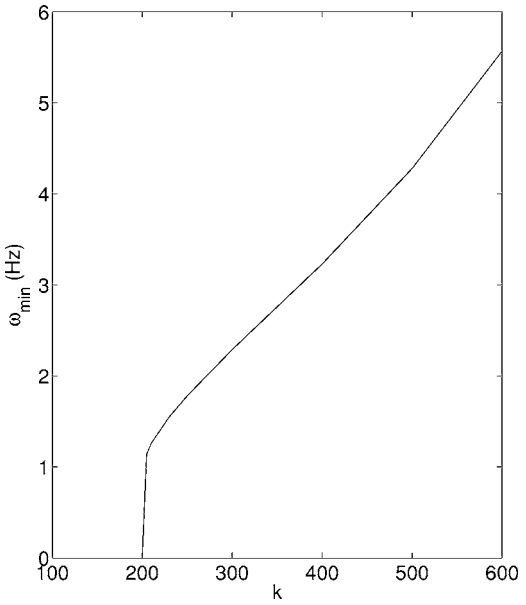

Fig. 9 Minimum operational frequency versus *k*

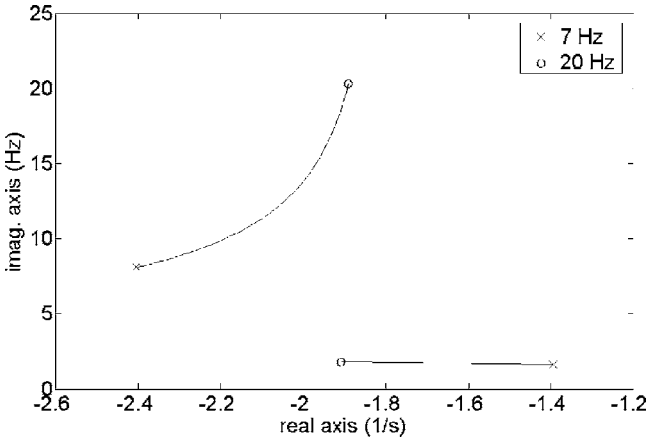

Fig. 10 Root locus plot of the poles of the transfer function of the PD with absolute absorber mass position and velocity, neglecting the dynamics of the actuator and filters

the absorber system and combined system are the same as listed, and the parameters of the electromagnetic actuator are $R=6.5\ \Omega$, $L=1.07$ mH, $K_f=5.56$ N/A, and $K_b=5.58$ V/m. The point $[K_p\ K_i]=[0\ 0]$ (indicated with an asterisk) can be the starting point for the D-subdivision stability analysis: it represents zero control force or, equivalently, a passive absorber whose stability (both the absorber system and the combined system) is guaranteed. Moving from the point [0 0] in the K_i-K_p plane, the stability of the combined system is guaranteed as long as the imaginary axis is not crossed. This crossing happens at any point on the dotted line. The dotted line is obtained by plotting K_p versus K_i in Eqs. (23) and (24) by varying ω_c. These equations give the K_p and K_i values that make the combined system marginally stable. Therefore, the section of the absorber marginal stability (the solid line) that can be connected to the point [0 0] without crossing the dotted line corresponds to the stable region. This section is anywhere on the solid curve. Since no crossing exists between the two curves, the combined system is always stable.

Since the properties of the primary system can change depending on how the device is held, a variation of k in a range of 100–600 N/m was investigated. For values of k larger than 200 N/m, the combined system becomes unstable at low frequencies. Figure 9 shows the minimum operational frequency as a function of k while other parameters are kept fixed. The maximum operational frequency is still theoretically ∞. A variation of b in a range of 2–20 kg/s ($0.08<\zeta<0.85$) was investigated. The results show that the combined system is always stable. Finally, b_a was allowed to vary between 0.5 and 5 kg/s, since the damping comes from nonlinear sources of Coulomb friction and Eddy currents. Again, the combined system was observed to be always stable.

6 Transient Response of the Combined System

The transient response of the combined system determines the time needed to achieve vibration absorption and is especially important dealing with excitations with variable amplitude or frequency. In this section, we investigate the transient response of three different active vibration absorbers, proportional derivative (PD-DVA), PI-DVA, and DR. Having different characteristics, they all cancel vibration by making the absorber system mimic a mass–spring duo. To study the transient response of the three methods, poles of the transfer function between x and f_e are obtained. For simpler comparison, the dynamics of the actuator is neglected[5] and it is assumed that no filter is used.

6.1 PD Transient Response. The control force of a PD controller with position feedback is

$$f_c = K_p x_a + K_d \dot{x}_a \tag{25}$$

where K_p and K_d are the proportional and derivative gain coefficients, respectively, and $\dot{x}_a$ can be obtained by differentiating x_a. In order for the absorber system to mimic a resonator at the frequency of ω_e, K_p and K_d should be selected as

$$K_p = -m_a\omega_e^2 + k_a \quad \text{and} \quad K_d = b_a \tag{26}$$

With this K_p and K_d, the transfer function between x and f_c is

$$\frac{X(s)}{F_e(s)} = \frac{s^2+\omega_e^2}{Q(s)(s^2+\omega_e^2) - b_a\omega_e^2 s - k_a\omega_e^2} \tag{27}$$

where $Q(s)=ms^2+(b+b_a)s+k+k_a$. Figure 10 shows two of the four conjugate roots of the denominator of Eq. (30) as the excitation frequency ω_e is varied. The range of 7–20 Hz is plotted to facilitate comparison since all three active vibration absorbers are operational in this range.

It is not possible in many applications to obtain absolute measurements of the absorber's displacement and velocity, therefore a relative measurement with respect to the primary mass should be used. The control force of a PD controller with relative position feedback is

$$f_c = K_p(x_a - x) + K_d(\dot{x}_a - \dot{x}) \tag{28}$$

K_p and K_d are still obtained according to Eq. (26). The transfer function between x and f_c is

$$\frac{X(s)}{F_e(s)} = \frac{s^2+\omega_e^2}{(ms^2+bs+k+m_a\omega^2)(s^2+\omega_e^2) - m_a\omega_e^4} \tag{29}$$

As expected, this transfer function is identical to the transfer function of Eq. (1) if the k_a in Fig. 4 is replaced with a $m_a\omega_e^2$ variable spring. Two of the four conjugate roots of the denominator of Eq. (32) are shown in Fig 11. Compared to Fig 10, the vibration absorption is slower with relative position feedback.

[5]It is not difficult to show that the characteristic equation of the absorber system, after inserting the numerical values for the absorber and primary systems and the electromagnetic actuator, has an extra root at $a=4.9\times10^5\times\omega_e^{-2}$ where ω_e is in Hz and a has the units 1/s. This root is associated with the dynamics of the electromagnetic actuator and is sufficiently far from the imaginary axis in the 5–25 Hz frequency range to be neglected.

6.2 PI Transient Response. With the K_p and K_i given in Eq. (5), the transfer function between x and f_e is

$$\frac{X(s)}{F_e(s)} = \frac{s^2 + \omega_e^2}{Q(s)(s^2 + \omega_e^2) + (m_a\omega_e^2 b_a/k_a - b_a)s^3 + (m_a\omega_e^2 - k_a)s^2 - \omega_e^2 b_a s - k_a w_e^2} \tag{30}$$

The poles of the transfer function determine the transient response of the combined system. Figure 12 shows the place of two of the four conjugate roots of the denominator of Eq. (30) as the excitation frequency ω_e is varied.

6.3 DR Transient Response. As mentioned in the "Introduction," DR is a widely adopted active DVA design whose control law is decoupled from the primary system. The control force in DR with acceleration feedback is [25]

$$f_c = g\ddot{x}_a(t - \tau) \tag{31}$$

where g and τ are a gain delay value. Again forcing the characteristic equation of the absorber system to have two roots at $\pm j\omega_e$ gives [25]

$$g = \frac{1}{\omega_e^2}\sqrt{(b_a\omega_e)^2 + (m_a\omega_a^2 - k_a)^2} \tag{32}$$

$$\tau = \frac{1}{\omega_e}[\text{atan2}(b_a\omega_e, m_a\omega_e - k_a) + 2(l-1)\pi], \quad l = 1,2,\cdots \tag{33}$$

We always set $l=1$ in order to obtain the widest operational frequency range and the smallest settling time of DR. An analytical and experimental comparison between PD and DR performance is provided in Ref. [22]. This work is mainly focused on the effects of the electromagnetic actuator on the PD and DR controller and comparison of DR and PD operational frequency ranges. Here, we focus on the transient response of the DR. The transfer function between x and f_e is

$$\frac{X(s)}{F_e(s)} = \frac{N(s)}{D(s)} = \frac{P(s)}{P(s)Q(s) - (b_a s + k_a - gs^2 e^{-\tau s})(b_a s + k_a)} \tag{34}$$

where $P(s) = m_a s^2 + b_a s + k_a - gs^2 e^{-\tau s}$ is the characteristic equation of the absorber system and g and τ are known from Eqs. (26) and (27). The infinite poles and zeros of the transfer function, other than the two zeros at $\pm j\omega_e$, determine the transient response of the DR. In Ref. [26,27], a modified Nyquist criterion is used to obtain the real value of the closest roots of the denominator, with slight variations for DR with displacement feedback. This value is used to study the transient response of the combined system and is kept as small as possible (far from imaginary axis). However, a root of the denominator close to the imaginary axis does not always guarantee a slow response, since there might be a zero located close to the pole. A small value of the transfer function at the dominant pole can be an indicator of a root close the dominant pole. However, both real and imaginary values of the dominant pole are required to calculate the transfer function value. In this work we obtain the real and imaginary values of the zeros and poles of Eq. (29) numerically, as explained in the Appendix. Figure 13 shows the first four branches of the poles and the first branch of the zeros, excluding the two roots at $\pm j\omega_e$, of Eq. (29) that are closest to the imaginary axis as the excitation frequency ω_e varies. From this plot, at $\omega_e = 7.1$ Hz the pole on the third branch is located at $-0.05 + 114j$ and is the closest pole to the imaginary axis. However, a zero is located close to this pole which makes this pole indominant. This example also shows that even though at 7.1 Hz the absorber has a large settling time,[6] because of the close root of the characteristic equation of the absorber system ($P(s)$) to the imaginary axis, the combined system can have a small settling time. Generally speaking, this surprising behavior happens in systems with $\omega_{\text{na}} = \sqrt{k_a/m_a} \gg \omega_n = \sqrt{k/m}$; as happens in the hand-held device with $\omega_{\text{na}} \approx 9$ Hz and $\omega_n \approx 2$ Hz. A detailed analytical and experimental comparison between PD and DR performance is provided in Ref. [22].

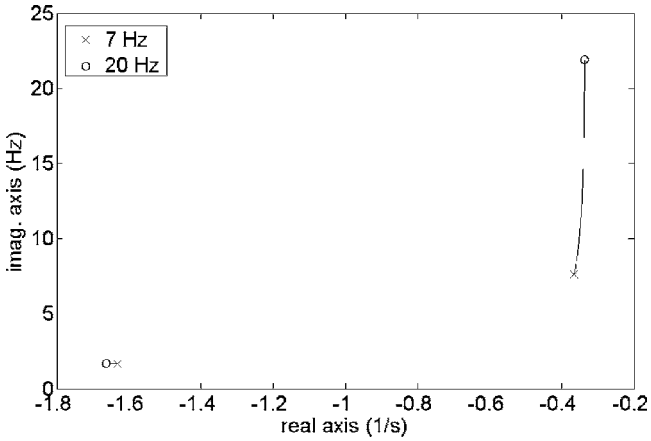

Fig. 11 Root locus plot of the poles of the transfer function of the PD with relative absorber mass position and velocity, neglecting the dynamics of the actuator and filters

7 Simulation Results

Simulations are performed by MATLAB Simulink using the properties of the combined system and actuator as described in Secs. 4 and 5

7.1 Absorber System. The absorber mass–spring–damper trio is considered first. Figure 14(*a*) shows the free vibration of the trio with no control force, which is clearly dissipative and stable. To make the trio marginally stable with two roots crossing the imaginary axis at $\pm j\omega_a = \pm j2\pi 10$, the PI control parameters K_p and K_i are calculated according to Eqs. (11) and (12) and the PI control force is applied to the absorber mass, resulting in a 10 Hz resonator (Fig. 14(*b*)). In Fig. 14(*c*) the tuning frequency is changed from 15 Hz to 7.5 Hz by changing the control parameters K_p and K_i, and the response of the system is observed. The PI-DVA becomes tuned to 7.5 Hz after a very short settling time (too small to be observable in the graph). The very small settling time required for the PI-DVA is associated with the actuator dynamics and filters used.

7.2 Combined System. A PI-DVA can completely cancel the primary system motion provided it is properly tuned to the excitation frequency. Figure 15(*a*) shows complete vibration suppression is achieved at 10 Hz excitations. Similar results can be plotted for other frequencies. Since the probe is hand-held, the amplitude of the excitation force can vary. Figure 15(*b*) shows the performance of the PI-DVA excitation with variable amplitude

[6]The characteristic equation of the absorber system of the DR, $P(s)$, has infinitely many roots. Therefore a DR absorber, unlike PI-DVA, is similar to a mass-spring system only after a settling time. This settling time is studied in Ref. [27] and should be distinguished from the settling time of the combined system, which can be observed in both PI and DR controllers.

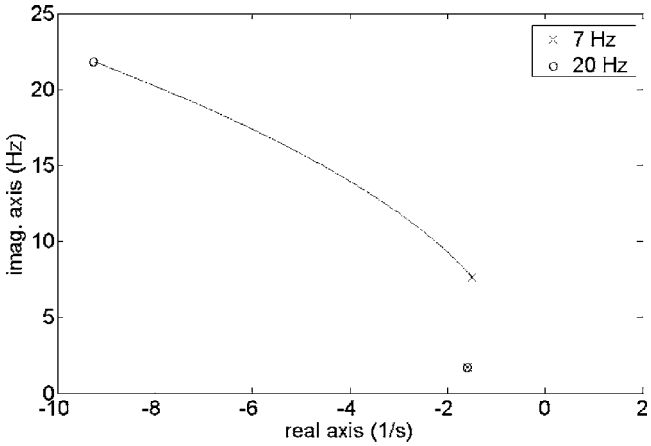

Fig. 12 Root locus plot of PI transfer function's poles, neglecting the dynamics of the actuator and filters

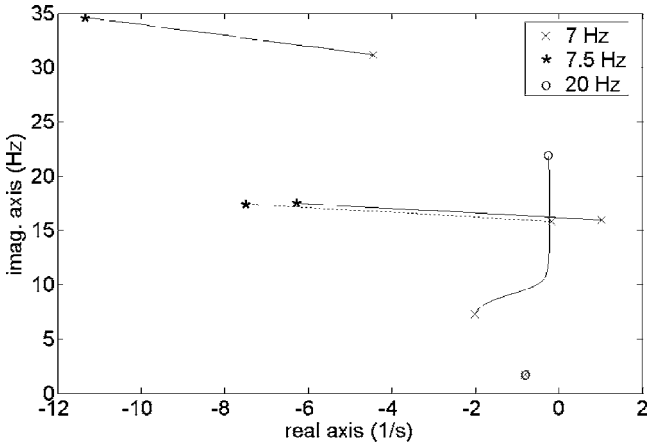

Fig. 13 Root locus plot of DR transfer function's poles and zeros, neglecting the dynamics of the actuator and filters

force, and Fig. 15(*c*) shows the performance with swept-sine excitation. There is a tradeoff between the rate of sweep (and therefore time required to cover the 5–25 Hz frequency range) and the vibration absorption performance.

The operational frequency range obtained in Sec. 5, and the transient response of the combined system with PD, PI, and DR obtained in Sec. 6, are verified by the simulation results.

8 Experimental Results

8.1 Absorber System. PI-DVA makes the stable absorber system marginally stable by placing two poles of the characteristic equation of the absorber system on the imaginary axis. This marginal stability was shown in the simulation results (Fig. 14). This resonance behavior of the absorber system is the key aspect of the vibration absorption and is investigated experimentally in this section.

Results of a free vibration test on the actual device with an approximately 3 mm absorber mass initial displacement are shown in Fig. 16(*a*). The system is clearly damped and vibrates approximately 1.5 cycles before it dissipates all energy. Figure 16(*b*) shows the lowpass filtered acceleration of the absorber mass when the control parameters K_p and K_i are tuned to 5 Hz. The vibration becomes slightly damped after $t=4$ s because of the uncertainties and nonlinearities in the absorber parameters. In Fig. 16(*c*) the tuning frequency is changed from 4.3 Hz to 2.7 Hz by changing the control parameters K_p and K_i at approximately t

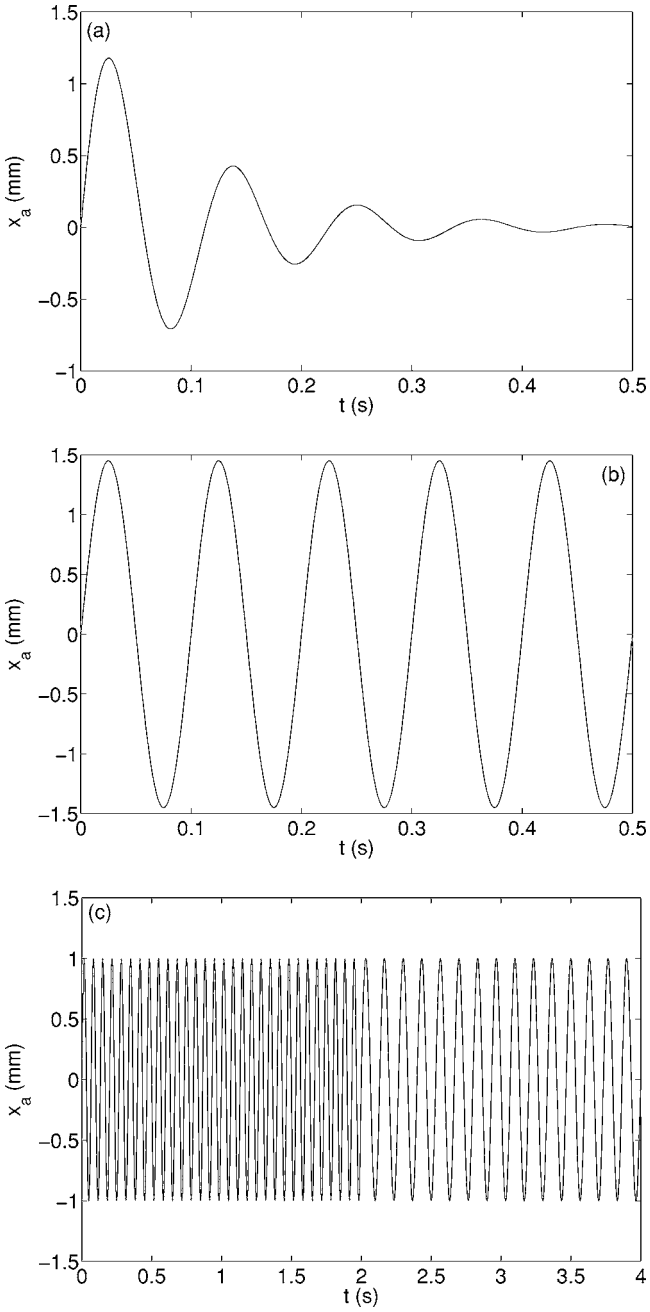

Fig. 14 (*a*) Free vibration of the absorber mass; (*b*) vibration of the absorber mass with the PI controller tuned to 10 Hz; (*c*) vibration of the absorber mass with the PI controller whose resonance frequency is changed from 15 Hz to 7.5 Hz at $t=2$ s

$=2.5$ s. The amplitude of vibration after tuning to 3 Hz is different from the amplitude of vibration before tuning to 3 Hz because of the initial conditions.

8.2 Combined System. A mechanical arm was built to hold the probe in order to perform repeatable and comparable experiments (Fig. 17). The arm has a stiffness of 140 N/m, mimicking the stiffness of the human arm holding the probe. An OPTOTRAK 3020 (NDI, Waterloo, Canada) tracker with a measurement rate of 500 Hz is used to track the motion of the probe. The OPTOTRAK is only used to investigate the performance of the vibration absorber and is not used as a sensor in the vibration absorption control algorithm. Figure 18 shows the vibration of the device

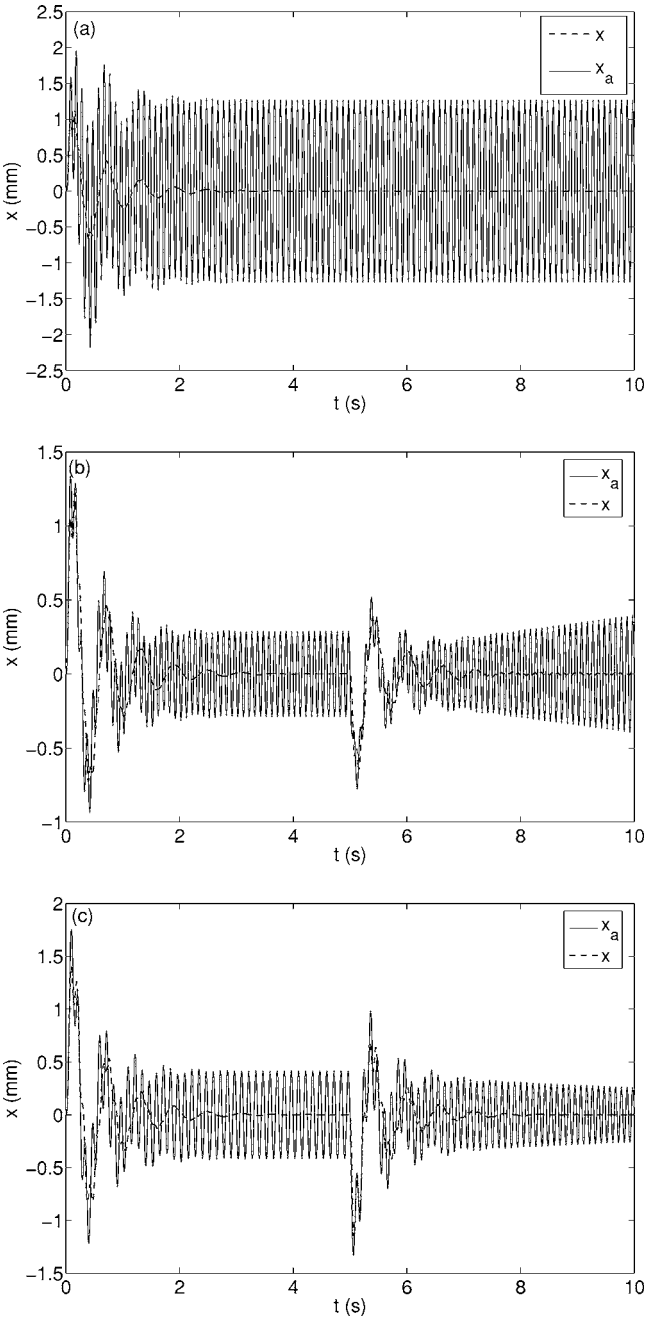

Fig. 15 Combined system simulation results: (*a*) vibration of the hand-held device and the absorber mass at 10 Hz excitation; and (*b*) vibration of the hand-held device at 10 Hz. The amplitude of excitation is a constant 1 N for $t=0-5$ s and is increased linearly from 0.5 N at $t=5$ s to 1.5 N at $t=10$ s; and (*c*) vibration of the hand-held device with a swept-sine excitation. Excitation frequency is a constant 8 Hz for $t=0-5$ s and is decreased linearly from 8 Hz at $t=4$ s to 16 Hz at $t=10$ s.

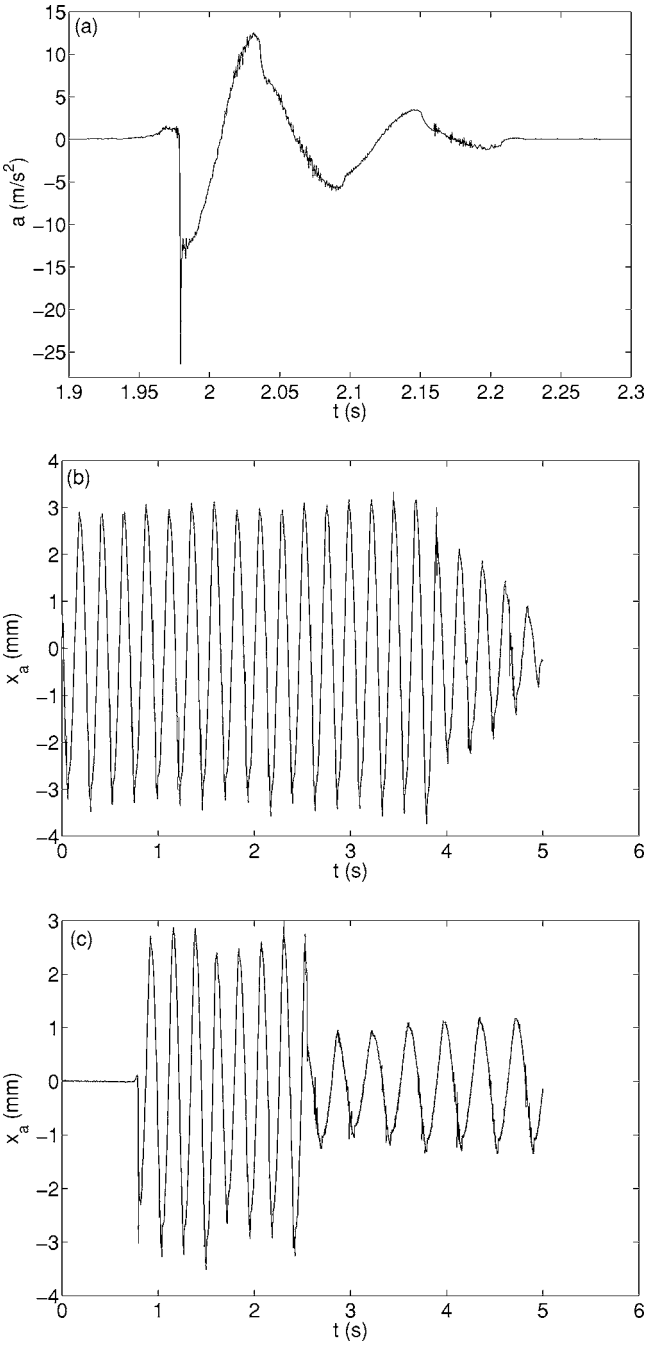

Fig. 16 (*a*) Free vibration experiment on the absorber system with no control force (*b*) vibration of the absorber mass controlled with PI tuned to 5 Hz; and (*c*) vibration of the absorber mass controlled with PI tuned to 4.3 Hz for $t=0-2.6$ s and to 2.7 Hz for $t=2.6-5$ s

before and after active vibration absorption at different frequencies. 15 dB, 28 dB, and 17 dB vibration absorption is achieved at 5 Hz, 10 Hz, and 15 Hz, respectively.

To determine the ability of the probe to absorb forces with variable amplitude, two experiments with and without active vibration absorption are done. In these experiments, the tissue excitation amplitude is increased from 1.7 mm to 2 mm at $t=2$ s (Fig. 19(*a*)). The amplitude of vibration is increased from 0.73 mm to 1 mm without vibration absorption and from 0.11 mm (16 dB vibration absorption) to 0.14 mm (17 dB vibration absorption) with vibration absorption. The experiment shows an increase in the attenuation level when the excitation force is increased because of the absorber system model errors (approximating nonlinear dampings with viscous damping). Figure 19(*b*) shows the results of two experiments performed with and without active vibration absorption (dashed curve and solid curve respectively). The first 2 s represent a constant amplitude, constant frequency excitation at 8 Hz. At $t=2$ s the excitation frequency starts to increase linearly from 8 Hz to 16 Hz in 5 s. The absorption performance deteriorates with increasing excitation frequency

Fig. 17 The hand-held device held by the mechanical arm

(from 16 dB at the beginning of the sweep to the 6 dB at its end) mainly because the amplitude of probe vibration decreases with increasing frequency, and Coulomb friction predominates.

Held by the mechanical arm, vibration absorption with the PI was performed from frequencies as low as 3 Hz to a maximum of 20 Hz. Vibration absorption below 3 Hz cannot be achieved because the amplitude of vibration of the absorber mass becomes larger than the absorber actuator's stroke, although the system is stable. Above 20 Hz, the amplitude of vibration of the device becomes too small, about 0.15 mm, to cancel. The cancelation of such small vibration is difficult mainly because of the Coulomb friction in the absorber. Due to the existence of Coulomb friction in the absorber part, the difference between the settling times of the PD, PI, and DR in the experimental results was not significant.

In Fig. 20, the probe is held by a human operator on human tissue (the forearm of another human subject). In this experiment, the vibration absorber decreases the peak-to-peak motion from approximately 1.28 mm to 0.13 mm. Because the probe is held by hand and applies a slightly uneven pressure to the tissue, a net motion at a low 2 Hz frequency (compared to the 10 Hz vibration frequency) is seen. This is a rigid body motion where both the vibrating forearm and hand-held probe move together and no vibration absorption is required for this vibration.

9 Discussion

The PI-DVA controller for the hand-held VE device is shown in theory, simulations, and experiments to offer significant vibration absorption over a useful range of frequencies. It also produces fast response times to changes in the excitation frequency or amplitude.

The PI controller is a faster alternative to the PD controller. However, the integration to obtain velocity from acceleration should be performed by exploiting a high-pass filter, which may not completely eliminate accumulation of error. No accumulation of error over long periods of time was observed in our device. The hand-held device is expected to operate for short periods of time, roughly 10 s for each elastogram, so accumulation of error is not expected to be a problem.

The PI-DVA with the primary system, absorber system and actuator properties described in this work provides, theoretically, an operational frequency range from zero to infinity. The main advantage of PI-DVA over PD and DR, for the particular application

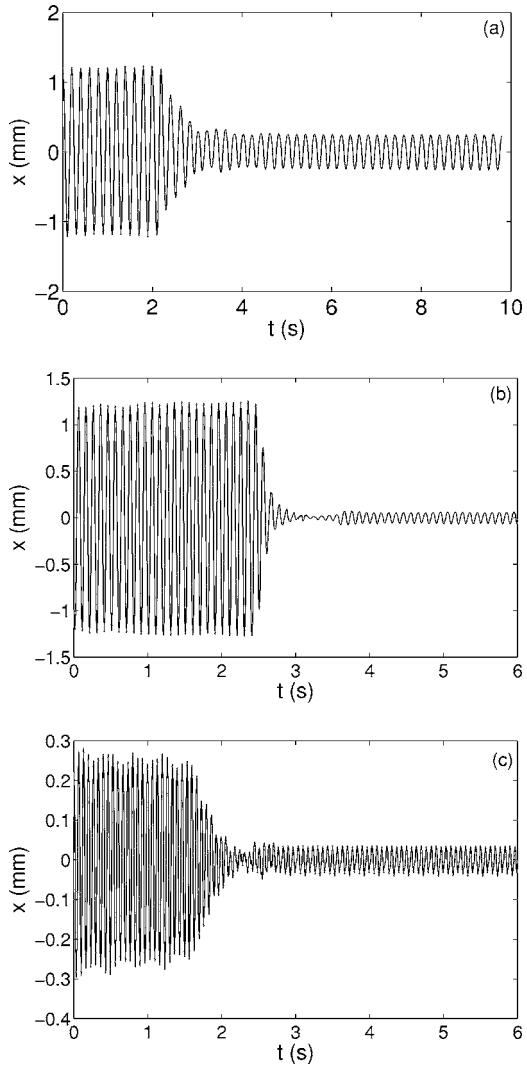

Fig. 18 Vibration absorption experiments at three different frequencies: (*a*) 5 Hz; (*b*) 10 Hz; and (*c*) 15 Hz

of the hand-held device, is a faster response at most frequencies. Fast vibration absorption is critical in the device because of the presence of variable excitation amplitude, since the probe is hand held, and variable frequency. Remanufacturing the device with a smaller mass, m, results in $\omega_{\mathrm{na}} \approx \omega_n$. Holding the device with a stiffer arm also makes ω_{na} and ω_n closer to each other. With these new parameters, it can be shown, again using an analysis similar to that of Sec. 6, that PI is much faster than DR over the whole operational frequency range.

With the PI-DVA method, only one feedback sensor is required. However, an extra feedback from the primary system can better the performance against uncertainties in the absorber system properties, as shown in Refs. [28,29]. By replacing the bushings with linear bearings, the performance of the vibration absorber should also be improved by reducing Coulomb friction.

Currently, no feed-forward scheme that uses the information about the future frequency of excitation, in the swept-sine excitation, is exploited in the control method. By introducing such a feed-forward scheme in the control algorithm, vibration absorption performance may also be improved. This feed-forward scheme may also be complemented by considering the electrical current sent to the primary actuator, which approximates the excitation force.

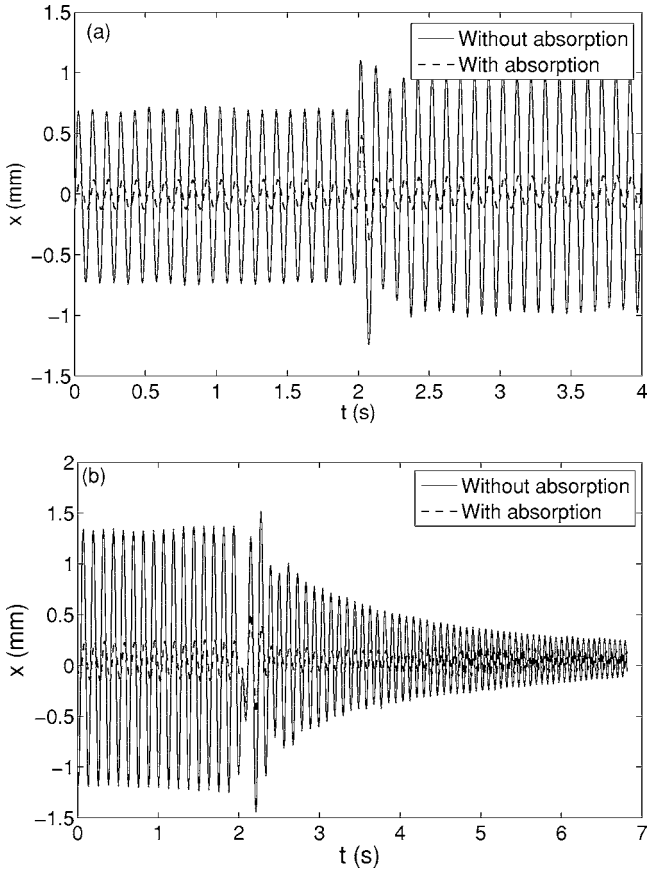

Fig. 19 Vibration absorption experiments: (*a*) the amplitude of excitation is changed from 1.7 mm to 2 mm at $t=2$ s; (*b*) the excitation frequency is 8 Hz for $t=0-2$ s; and is increased linearly to 16 Hz in 5 s

10 Conclusion

A PI-DVA control algorithm is suitable for a hand-held device for vibro-elastography using an electromagnetic actuator to apply the control force. Practically, the control algorithm requires only one feedback from the system, the acceleration of the absorber mass. The integration required to obtain the velocity data can be safely performed with the highpass filter since the device operates over short periods of time. The PI controller is a good choice for the hand-held device since it provides a sufficiently wide range of operation and fast response to changes in the excitation amplitude and frequency. The PI-DVA is shown to cancel vibrations faster than PD and DR. Compared to DR, however, the PI-DVA uses two acceleration and velocity feedbacks. The quality of the velocity data, which is obtained by integrating accelerometer data, can also affect the performance of the PI-DVA. This is especially important if the active vibration absorber is required to work for long periods of time.

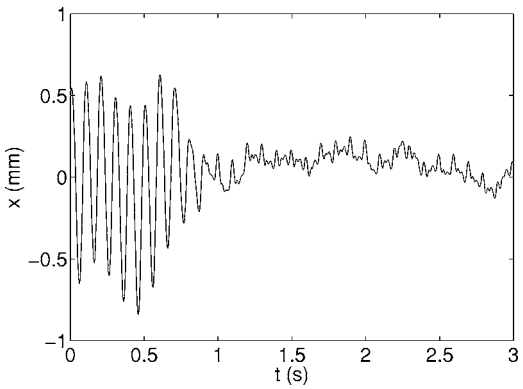

Fig. 20 Probe vibration for experiments with a human operator on real tissue. The vibration absorber is turned on at $t=0.7$

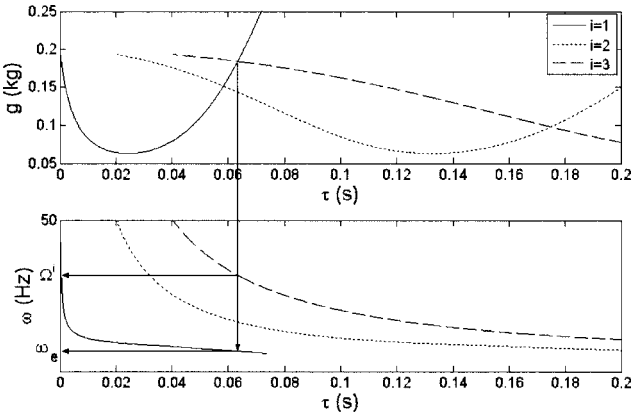

Fig. 21 Ω^i for $i=3$ and its corresponding ω_e

The analysis of the transient response of the combined system with a DR absorber also provides guidance for DR design. It also gives insight into the roots of the combined system, which can help a designer to choose among PD, PI, or DR controllers for a given vibration absorption application. Given a functioning device, work is now underway on clinical applications of VE.

Acknowledgment

This research was supported in part by the Natural Sciences and Engineering Research Council of Canada.

Appendix

Both the numerator and denominator of Eq. (29) have infinitely many roots and it is not easy to make the numerical method converge to the desired root. In order to find these zeros and poles, one point from each branch is required first. This point can be the crossing of each branch with the imaginary axis. This crossing is named Ω^i where i refers to ith branch. First we explain how this crossing can be found for branches of zeros. A typical root–locus plot of the DR for a given τ, as g varies, can be found in Ref. [22]. The crossing of the ith branch from the infinite branches of the plot with the imaginary axis can be achieved by obtaining g_i and τ_i from Eqs. (26) and (27) with $l=i$. By plotting g_i versus τ_i and g_1 versus τ_1 in the same figure as ω_e varies, this crossing point and its corresponding ω_e can be found from the intersection of the two curves (Fig. 21). The crossing of the branches of poles of Eq. (29) with the imaginary axis can be found similarly.

Given the crossing of each branch of the zeros and poles of Eq. (29) with the imaginary axis, Ω^i, and its corresponding ω_e, the root–locus plot can be obtained by increasing ω_e by a small amount and using the place of the root at the previous frequency as the initial guess for the numerical method.

References

[1] Reeves, M., Newcomb, P., and Marcus, P., 1995, "Determinants of Breast Cancer Detection Among Wisconsin (United States) Women," Cancer Causes Control, **6**, pp. 103–111.
[2] Kallel, F., and Bertrand, M., 1996, "Tissue Elasticity Reconstruction Using Perturbation Method," IEEE Trans. Med. Imaging, **15**, pp. 299–313.
[3] Turgay, E., MacIntosh, S., Rohling, R., and Salcudean, S., 2003, "Parameter Identification of Tissue Lumped Models Based on Sequences of Ultrasonic Strain Images," *Proceedings 2nd International Conference Ultrasonic Meas., Imaging Tissue Elasticity*, Corpus Christi, TX, October, p. 9.
[4] Turgay, E., Rohling, R., and Salcudean, S., 2006, "Identifying the Mechanical

Properties of Tissue by Ultrasound Strain Imaging," Ultrasound Med. Biol., **32**(2), pp. 221–235.
[5] Turgay, M., Salcudean, S. E., and Rohling, R., 2004, "Method for Imaging the Mechanical Properties of Tissue," Provisional Patent No. 2457376, February.
[6] Karnopp, D., 1995, "Active and Semi-Active Vibration Absorption," ASME J. Mech. Des., **117**, pp. 177–185.
[7] Korenev, B., and Reznikov, L., 1993, *Dynamic Vibration Absorbers: Theory and Technical Applications*, Wiley, New York.
[8] Sun, J., Jolly, M., and Norris, M., 1995, "Passive, Adaptive and Active Tuned Vibration Absorbers—A Survey," J. Vibr. Acoust., **117**, pp. 234–242.
[9] Jalili, N., 2002, "A Comparative Study and Analysis of Semi-Active Vibration-Control Systems," ASME J. Vibr. Acoust., **124**(4), pp. 593–605.
[10] Thomson, W., and Dahleh, M., 1998, *Theory of Vibration with Applications*, 5th ed., Prentice–Hall, Englewood Cliffs, NJ.
[11] Zuo, L., and Nayfeh, S., 2005, "Optimization of the Individual Stiffness and Damping Parameters in Multiple-Tuned-Mass-Damper Systems," ASME J. Vibr. Acoust., **127**, pp. 77–83.
[12] Wang, P., and Cheng, C., 2005, "Design of Vibration Absorbers for Structures Subject to Multiple-Tonal Excitations," ASME J. Vibr. Acoust., **128**, pp. 106–114.
[13] Bajaj, A., Chang, S., and Johnson, J. M., 1994, "Amplitude Modulated Dynamics of a Resonantly Excited Autoparametric Two Degree-Of-Freedom System," Nonlinear Dyn., **5**, pp. 433–457.
[14] Vyas, A., and Bajaj, A., 2001, "Dynamics of Autoparametric Vibration Absorbers Using Multiple Pendulums," J. Sound Vib., **246**, pp. 115–135.
[15] Golysheva, E., Babitsky, V., and Veprik, A., 2004, "Vibration Protection for an Operator of a Hand-Held Percussion Machine," J. Sound Vib., **274**, pp. 351–367.
[16] Lim, K. B., Maghami, P. G., and Joshi, S. M., 1992, "Comparison of Controller Designs for an Experimental Flexible Structure," IEEE Control Syst., **12**, pp. 108–118.
[17] Asami, T., and Nishihara, O., 2002, "H_2 Optimization of the Three-Element Type Dynamic Vibration Absorbers," ASME J. Vibr. Acoust., **124**(4), pp. 583–592.
[18] Flipovic, D., and Schroder, D., 1998, "Bandpass Vibration Absorber," J. Sound Vib., **214**(3), pp. 553–566.
[19] Jalili, N., and Olgac, N., 1998, "Optimum Delayed Feedback Vibration Absorber for MDOF Mechanical Structures," *Proceedings IEEE Conference Decision, Control*, Tampa, FL, Vol. 4, pp. 4734–4739.
[20] Chen, W., Wang, X., Sun, C., Devine, F., and De Silva, C., 2003, "Active Vibration Control With State Feedback in Woodcutting," J. Vib. Control, **9**(6), pp. 645–64.
[21] Olgac, N., and Holm-Hansen, B., 1993, "New Direction in Active Vibration Absorption: Delayed Resonator," *Proceedings ASME Symposium Mechatron.*, New Orleans, LA, pp. 15–20.
[22] Elmali, H., Renzulli, M., and Olgac, N., 2000, "Experimental Comparison of Delayed Resonator and PD Controlled Vibration Absorbers Using Electromagnetic Actuators," ASME J. Dyn. Syst., Meas., Control, **122**, pp. 514–520.
[23] Bhattacharyya, S., Chapellat, H., and Keel, L., 1995, *Robust Control: The Parametric Approach*, Prentice-Hall, Englewood Cliffs, NJ.
[24] Ogata, K., 2002, *Modern Control Engineering*, 4th ed. Prentice-Hall, Uppder Saddle River, NJ.
[25] Olgac, N., Elmali, H., Hosek, M., and Renzulli, M., 1997, "Active Vibration Control of Distributed Systems Using Delayed Resonant With Acceleration Feedback," ASME J. Dyn. Syst., Meas., Control, **119**, pp. 380–389.
[26] Olgac, N., and Hosek, M., 1997, "Active Vibration Absorption Using Delayed Resonator With Relative Position Measurement," J. Vibr. Acoust., **119**, pp. 131–136.
[27] Olgac, N., and Holm-Hansen, B., 1995, "Design Consideration for Delayed-Resonator Vibration Absorbers," J. Eng. Mech., **121**(1), pp. 80–89.
[28] Renzulli, M., Ghosh-Roy, R., and Olgac, N., 1999, "Robust Control of the Delayed Resonator Vibration Absorber," IEEE Trans. Control Syst. Technol., **7**(6), pp. 683–691.
[29] Hosek, M., and Olgac, N., 2002, "A Single-Step Automatic Tuning Algorithm for the Delayed Resonator Vibration Absorber," IEEE/ASME Trans. Mechatron., **7**(2), pp. 245–455.